Stretchable Liquid Metal E-Skin for Soft Robot Proprioceptive Vibration Sensing

Zihan Wang, Kai-Chong Lei, Huaze Tang, *Graduate Student Member, IEEE*, Yang Luo, Hongfa Zhao, Peisheng He, Wenbo Ding, *Member, IEEE*, and Liwei Lin, *Member, IEEE*

***Abstract*—Vibration perception can help robots recognize their dynamic states to explore the surrounding environment. However, the intrinsic stretchability of soft robots poses challenges to integrating vibration sensors. This study introduces an innovative stretchable electronic skin (e-skin) that facilitates vibration proprioception in soft robots. Constructed with a thickness of approximately 0.1 mm, this ultrathin e-skin is produced using a screen-printing technique with liquid metal particles (LMPs), incorporating a kirigami design for seamless integration. The e-skin works by the triboelectric nanogenerator-based sensing mechanism, which transduces mechanical vibration into an electrical signal without an external power source. By analyzing the vibration signals generated by the dynamic motions of soft robots, the e-skin shows a wide range of applications. From the vibration signal of the soft robotic finger's sliding motion, 17 different textures can be distinguished with 99% accuracy. Furthermore, analysis of the vibration signal from a soft robotic gripper's swinging motion enables the estimation of both the type and weight of grains inside the container it grips, achieving accuracies of 97.7% and 95.3%, respectively. As such, this work presents a new approach to realizing the vibration proprioception of soft robots, thereby broadening the applications of dynamic proprioception in soft robotics.**

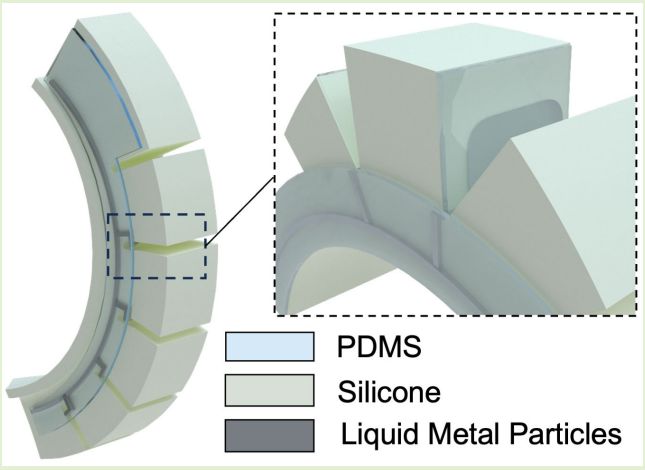

***Index Terms*— Liquid metal, soft robotic sensor, stretchable sensor, vibration sensing.**

Manuscript received 15 March 2024; accepted 21 April 2024. Date of publication 29 April 2024; date of current version 31 May 2024. This work was supported in part by Shenzhen Key Laboratory of Ubiquitous Data Enabling under Grant ZDSYS20220527171406015, in part by the National Natural Science Foundation of China under Grant 62104125 and Grant 62311530102, in part by Guangdong Innovative and Entrepreneurial Research Team Program under Grant 2021ZT09L197, in part by Shenzhen Science and Technology Program under Grant JCYJ20220530143013030, in part by the Tsinghua Shenzhen International Graduate School-Shenzhen Pengrui Young Faculty Program of Shenzhen Pengrui Foundation under Grant SZPR2023005, and in part by Meituan. An earlier version of this paper was presented in part at the International Conference on Robotics and Automation, London, U.K., May 2023 [DOI: 10.1109/ICRA48891.2023.10160790]. The associate editor coordinating the review of this article and approving it for publication was Dr. Yang Yang. *(Zihan Wang and Kai-Chong Lei are co-first authors.) (Corresponding author: Wenbo Ding.)*

Zihan Wang is with the Tsinghua–Berkeley Shenzhen Institute, Tsinghua Shenzhen International Graduate School, Tsinghua University, Beijing 100084, China, and also with the Department of Mechanical Engineering, University of California at Berkeley, Berkeley, CA 94720 USA.

Kai-Chong Lei, Huaze Tang, Yang Luo, Hongfa Zhao, and Wenbo Ding are with the Tsinghua–Berkeley Shenzhen Institute, Shenzhen International Graduate School, Tsinghua University, Beijing 100084, China (e-mail: ding.wenbo@sz.tsinghua.edu.cn).

Peisheng He and Liwei Lin are with the Department of Mechanical Engineering, University of California at Berkeley, Berkeley, CA 94720 USA.

This article has supplementary downloadable material available at https://doi.org/10.1109/JSEN.2024.3392837, provided by the authors.

Digital Object Identifier 10.1109/JSEN.2024.3392837

I. Introduction

VIBRATION sensation is essential for robotic applications, as it enables robots to capture subtle motion profiles and interact with the environment intelligently. By incorporating vibration sensors, robots can detect the slippage of delicate objects [1], distinguish surface textures [2], and maintain their operation stabilization [3]. As technology evolves, emerging soft robots have become essential complements to rigid robots, leading to more adaptable and versatile robots [4]. However, the existing inflexible [5] or flexible but nonstretchable vibration sensors [6] are mechanically mismatched with the stretchable soft robots [7]. Therefore, deploying vibration sensors on soft robots without compromising their flexibility and dexterity is challenging.

Nowadays, electronic skins (e-skins), inspired by multiple senses of biological skin, have been engineered for seamless integration on soft robots to provide diversified sensing capabilities [8], [9]. The mechanical properties of stretchable e-skin, known for its adaptability to the soft robots' body, allow minimal interference on soft robots [10]. Regarding proprioceptive sensing, e-skin empowers soft robots to perceive their self-states in various sensing mechanisms [11], [12]. The resistive-based e-skin is stable and accurate in measuring soft robots' static bending angles [13]. However, the resistance hysteresis limited the reading frequency [14], which

is unfavorable for vibration sensing. Although fiber Bragg gratings can provide a fast and accurate vibration sensing [15], the complex and expensive optical signal modulation equipment and the fiber's limited stretchability prevent them from being widely adopted in soft robots. Low-cost, flexible piezoelectric sensors advantageous in vibration sensing also have limited stretchability [16]. With large vibration sensing bandwidth [17], excellent stretchability [18], and low cost, triboelectric sensors are expected to be a promising candidate for vibration sensors. Nevertheless, efforts are needed to identify suitable fabrication techniques and design principles for triboelectric vibration sensors used in soft robots.

Previously, a triboelectric stretchable e-skin has been customized for soft robots' proprioceptive vibration sensing [19]. This article presents more comprehensive characterizations of the e-skin's vibration sensing performance and provides deeper insights into using the vibration signals for multifunctional robotic sensing. Two sensing tasks with one channel vibration signal have been accomplished [see Fig. 1(a)]. First, we demonstrate that vibration proprioception enables a soft robotic finger tactile sensing function, as the vibration frequency profile from the soft finger's sliding motion is used to recognize 17 surface textures with 99% accuracy. Moreover, we adopt the wavelet transform-based signal-processing algorithm to decouple the vibration signal of a soft gripper that swings the container, and use the decoupled signal features to simultaneously estimate content type and weight inside a container with 97.7% and 95.3% accuracy, respectively.

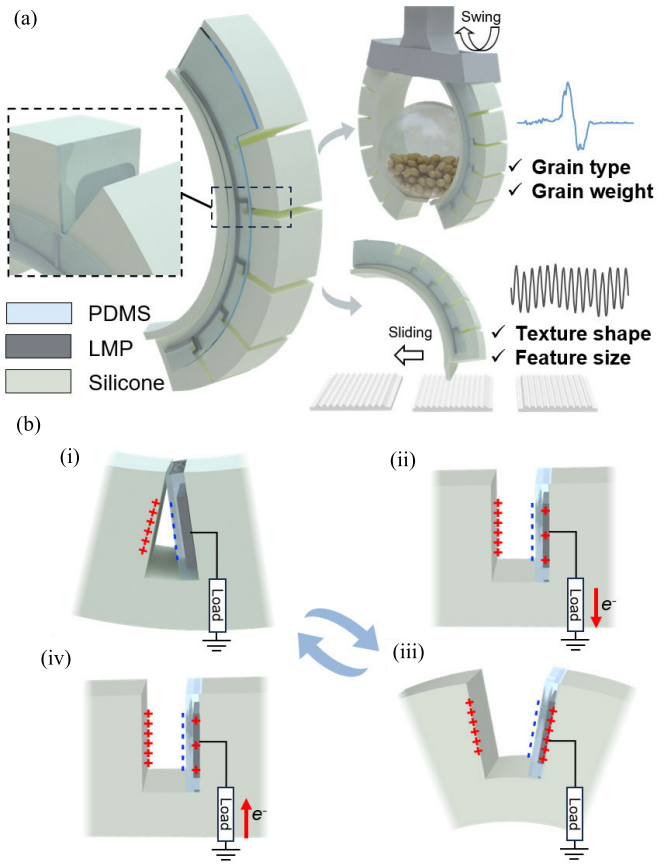

Fig. 1. (a) Vibration sensing e-skin-enabled soft robots with grain and texture properties estimation functions. (b) Close-up view of the air chamber gap within one triboelectric working cycle.

II. Methods

A. Sensing Mechanism of the E-Skin

The e-skin has four electrodes in parallel installed on four air-chamber intervals. For each interval between adjacent air-chamber walls, the liquid metal particles (LMPs) stretchable electrode with polydimethylsiloxane (PDMS) encapsulation is bonded to one side of the air-chamber wall, while the silicone air-chamber wall of the other side is untouched. As depicted in Fig. 1(b), after connecting the LMPs circuit to the ground through an external load resistor, the e-skin equipped on the soft robot forms a single-electrode mode TENG (SE-TENG) [20]. Note that the color representation of materials in Fig. 1(b) is consistent with Fig. 1(a).

The sensor's working cycle is analyzed from one period of the soft robot's vibration. As Fig. 1(b-i) exemplifies, initially, the soft robot's vibration motion bends adjacent air chambers to an inward position, the silicone layer contacts with the PDMS layer, and the PDMS gains negative triboelectric charges due to its higher affinity to negative charge [21], whereas the silicone is positively charged. As the soft robot relaxes to the position in Fig. 1(b-ii), the PDMS layer begins to separate from the silicone layer, and the potential difference leads to the flow of electrons from the LMPs electrode to the ground through the load resistor. The current flow continues until the soft robot bends to the most outward position shown in Fig. 1(b-iii), where the PDMS and silicone layer are most separated, and the system reaches electrostatic balance. Afterward, the soft robot starts to bend inward [see Fig. 1(b-iv)] as the PDMS layer approaches the silicone layer, and the electrons follow back to the LMPs electrode from the ground through the external load. The vibration of the soft robot is essentially the repetition of the contact-separation movement to generate an alternative current signal. The theoretical analysis and COMSOL multiphysics of the e-skin operating as SE-TENG are elaborated in supplementary note S1.

B. Fabrication Process of the E-Skin

Nontoxic room temperature liquid metal alloy eutectic gallium-indium (EGaIn) is an emerging material in stretchable sensor fabrication [22]. However, EGaIn has high surface energy (>600 mN/m) and poor wettability on polymers, which makes it difficult to be directly printed with fine features in the bulk form [23]. Dispersing bulk liquid metal in solvents to make LMPs ink can significantly reduce its high surface energy, which makes patterning circuits with fine details possible [24]. However, a nonconductive gallium oxide layer will form on the surface of LMPs due to the presence of oxygen in the air. Therefore, the printed circuit needs a sintering

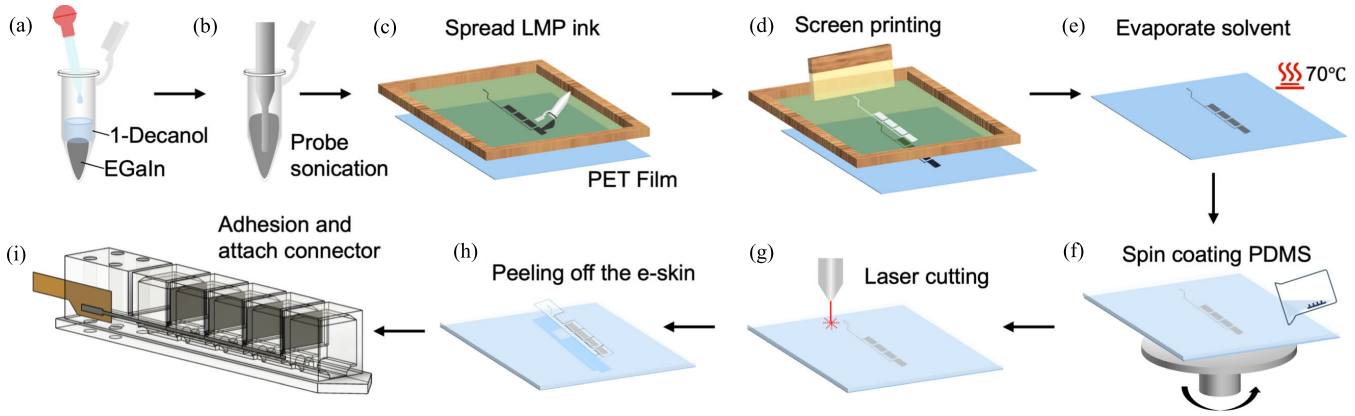

Fig. 2. Fabrication process of the e-skin. (a) Add regents to a centrifuge tube. (b) Disperse bulk liquid metal to from LMPs ink by probe ultrasonication. (c) Spread the LMPs ink on a printing screen. (d) Screen print the electrode on a PET releasing film. (e) Evaporate ink solvent. (f) Spin coat PDMS precursor. (g) Laser cutting e-skin's perimeter. (h) Peeling off e-skin from PET releasing film. (i) Attach FPC connector and adhere the e-skin to soft robot.

process, such as mechanical stress [25], laser exposure [26], or freeze-thaw [27], to break the oxidation layer and form interconnected conductive paths. Based on previous works, LMPs conductive ink and screen-printing techniques are combined to pattern the stretchable circuit. The detailed fabrication process is illustrated in Fig. 2.

The first step of the fabrication is to prepare the LMPs ink, a suspension liquid of micrometer-level EGaIn droplet, and solvent. Fig. 2(a) and (b) shows that 3 g EGaIn (Ga:In = 3:1 in weight, Dingguan Metal Inc.) and 0.415 g 1-Decanol (98%, Aladdin) are added to a centrifugal tube and a 3 mm diameter sonication probe (JY92-IIN) is inserted into the liquid compound to apply 150 W ultrasonic agitation for 3 min. Since the ultrasonic probing generates massive heat, the centrifugal tube is moved from 25 °C ambient temperature into a beaker with 0 °C ice-water compound during the ultrasonic agitation. For the best acoustic field distribution, the probe tip is positioned 1 mm above the interface between bulk EGaIn and 1-Decanol [28]. The diameters of dispersed LMPs are spherical with approximately 10 μm in diameter (Fig. S1). Afterward, the screen-printing technique is used to pattern the LMPs ink. At first, the LMPs ink is evenly spread on a 250 mesh-printing screen with a predesigned circuit pattern [see Fig. 2(c)]. Then, a rubber scraper blade is scraped on the printing screen to print the circuit pattern on a silicone oil-coated PET-releasing film [see Fig. 2(d)]. The printed PET film is then transferred to a 70 °C oven for 10 min to evaporate the volatile 1-decanol solvent in the LMPs ink [see Fig. 2(e)]. After evaporation, the PDMS precursor (PDMS base:curing agent = 10:1 in weight) is spin-coated on the PET film at 600 r/min for 20 s to form a 148 μm thick (Fig. S2) elastic substrate film [see Fig. 2(f)]. The PDMS film is cured in the 70 °C oven for 1 h, and the film is cut by CO_2 laser [see Fig. 2(g)] with kirigami cutting and folding line indicated in Fig. S3. The cut-out PDMS film and its encapsulated LMPs circuit are carefully peeled off from the PET film [see Fig. 2(h)]. The peeling-off procedure also completes the sintering process. The detachment of the PDMS substrate introduces interfacial stress to LMPs and forces the nonconductive oxidation layer to break and form conductive paths [29]. Fig. S4 shows the e-skin before and after the peeling-off procedure and the surface scanning electron microscope view of the LMPs circuit on the e-skin. The measurement of the e-skin's resistance under different strains by Keithley 2600B precision source meter and ZQ-990LB mechanical test instrument is depicted in Fig. S5. Finally, a flexible printed circuit (FPC) connector is attached to the e-skin, and the e-skin is bonded to a PneuNet [30] soft robot's body via Dragon Skin[1] 30 (Smooth-On, Inc.) platinum cure liquid silicone compounds, the same material as the soft robot's body, to finish the assembly. The images of 3-D printed molds for casting the soft robot and the soft robot equipped with the e-skin is illustrated in Fig. S6.

The screen-printing technique provides a low-cost LMPs patterning approach with high resolution and ideal reproducibility. Meanwhile, the design allows the e-skin to seamlessly fit the soft robot's air-chamber wall. A video recording of the sensor fabrication process is reported in our previous work [19].

III. Experiments

A. Vibration Response Characterization

To evaluate the vibration response of the e-skin, a vibration exciter is used to build an apparatus that mimics the vibration-induced contact-separation motions between the soft robot's air chamber walls. Fig. 3(a) shows a silicone block attached to the end-effector of the vibration exciter to mimic the side of soft robot's air-chamber wall without the e-skin attachment. Meanwhile, the e-skin attached to a fixed silicone block mimics the other side with the e-skin attachment. The silicone block is cast by Dragon Skin 30. A Keithley 6514 electrometer is used to record the e-skin's triboelectric output signals, and the vibration exciter's motion amplitude is set to 1 mm, consistent with the gap distance of the soft robot's adjacent air-chamber walls. For sinusoidal axial vibration, the relationship

[1]Trademarked.

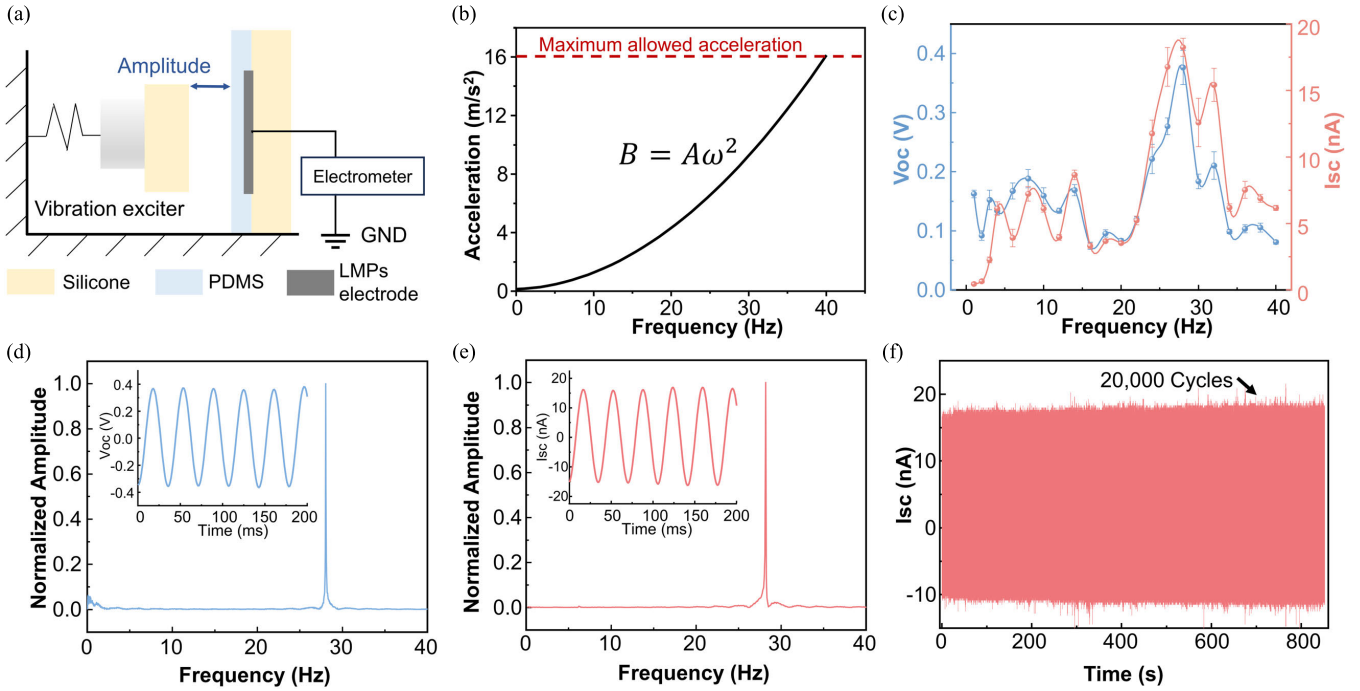

Fig. 3. (a) Diagram of the experiment setup for vibration response characterization. (b) Relationship between vibration frequency and acceleration at 1 mm vibration amplitude. (c) Peak values of open-circuit voltage (V_{oc}) and short-circuit current (I_{sc}) under in vibration frequencies from 1 to 40 Hz. (d) Short-circuit current and (e) open-circuit voltage signal waveform at 28 Hz vibration in frequency and time domain. (f) Durability measurement of the e-skin, where the short-circuit current (I_{sc}) is recorded for over 20 000 cycles at the frequency of 28 Hz.

between vibration frequency (ω) and acceleration (B) at a given 1 mm amplitude (A) is

$$B = A\omega^2. \tag{1}$$

Since the maximum allowed acceleration of the vibration exciter is 16 m/s^2, the vibration response characterization is implemented under 40 Hz [see Fig. 3(b)]. Fig. 3(c) plots peak values of the e-skin's open-circuit voltage and short-circuit current output under the vibration frequency range from 1 to 40 Hz, where the highest output occurs at 28 Hz. The short-circuit current and open-circuit voltage at 28 Hz vibration are shown in Fig. 3(d) and (e), respectively. The durability of the e-skin at 28 Hz vibration is tested by applying more than 20 000 contact-separation cycles, and the short-current output does not show significant degradation [see Fig. 3(f)].

B. Texture Recognition by Soft Robotic Finger's Vibration Proprioception

Conventionally, robots recognize surface textures by tactile sensing (Table S1), where sensors are directly in contact with samples [31]. However, contact-based tactile sensing may cause sensor abrasion in long-term usage. With the vibration proprioception, a soft robotic finger may achieve tactile sensing by sliding over samples. Since it is the soft robot's body instead of sensors that are in contact with external objects, sensor abrasion can be significantly reduced. Moreover, the soft robot is less harmful to surfaces made of fragile materials than rigid sensors.

To demonstrate the soft robots' vibration, proprioception can also be used for texture recognition, and we built a platform that drives a soft robotic finger slide-over texture sample. The soft robotic finger equipped with the e-skin is installed on the end-effector of a robotic arm (UR3, Universal Robots) that horizontally slides at a 50 mm/s constant speed. The distal end of the soft robotic finger is designed with a triangle-shaped fingertip [see Fig. 4(a)], which ensures that the fingertip can stay in contact with bulges and grooves on samples. The 3-D printed texture samples with five types of cross-sectional shapes (triangle, trapezoid, sawtooth, arch, and flat), as illustrated in Fig. 4(b), are used to evaluate the texture sensing performance. The feature size of nonflat texture shapes has four variations (W = 4, 5, 6, 8 mm). The 3-D printing models of all samples are shown in Fig. S7, where the dimension of all samples is 100 × 100 mm.

The signal-processing pipeline for texture recognition is drawn in Fig. 4(c). First, the triboelectric output of the e-skin is connected with a 100 MΩ sampling resistor to the ground. The voltage between the sampling resistor, which characterized the current output of the e-skin by Ohm's law, is recorded by the NI 9220 acquisition board. The schematic of the measurement circuit is illustrated in Fig. S8. Then, we use a 40 Hz low-pass filter to remove powerline noise in the data frames. The frequency domain profile of the denoised data frames is extracted by fast Fourier transform (FFT). Fig. 4(d) showcases the time data frames and frequency domain features of five samples with different textures. It can be observed that the frequency profiles of each texture are distinctive. The frequency profiles of all samples are shown in Fig. S9. Finally,

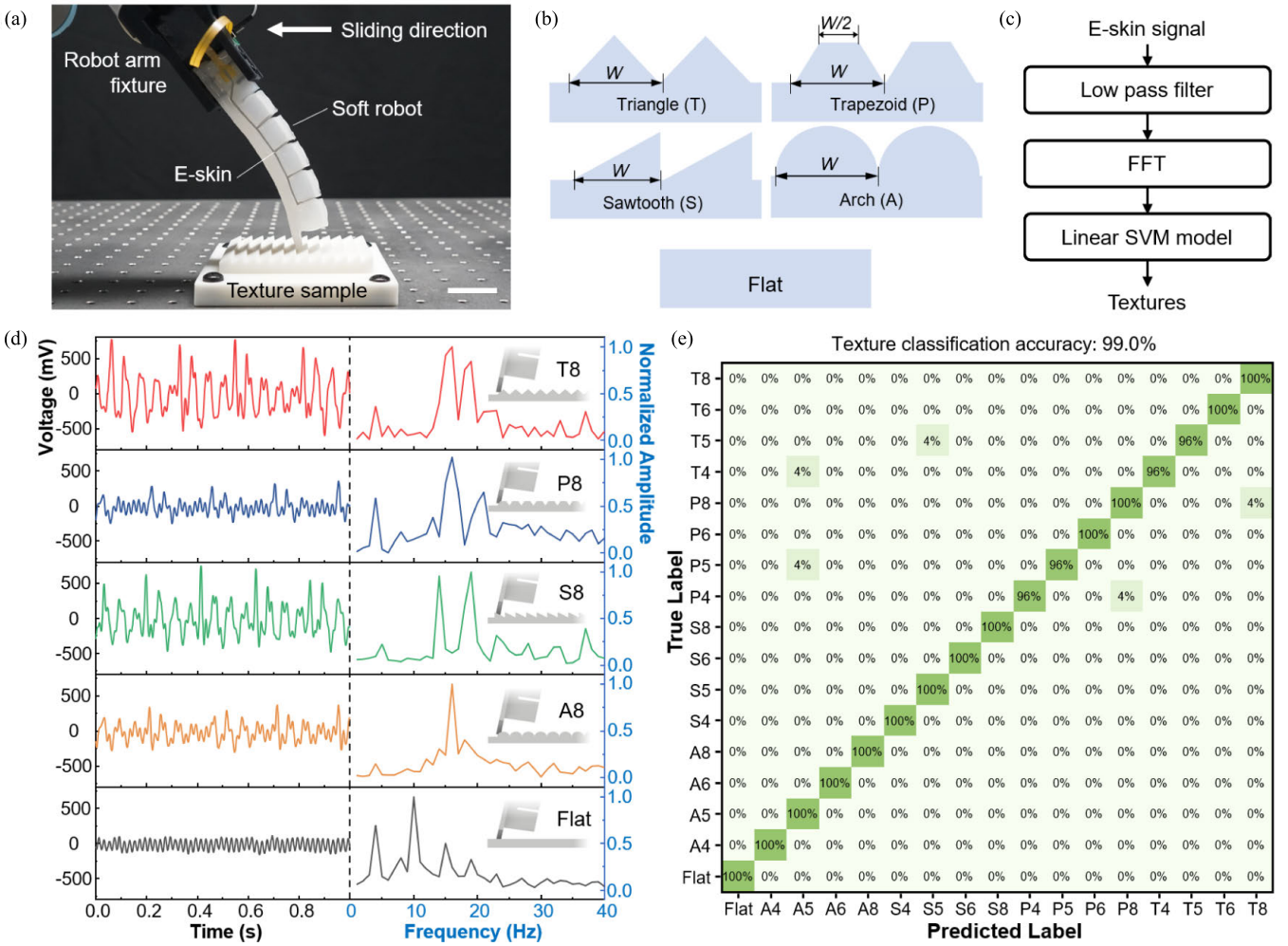

Fig. 4. (a) Soft robotic finger with triangular fingertip slide over texture sample (Scalebar: 25 mm). (b) Cross-section illustration and abbreviations of texture shapes, the notation "*W*" marks the definition of textures' feature sizes. (c) Signal processing pipeline. (d) E-skin's output in time and frequency domain of sliding five samples with different textures. (e) Confusion matrix of texture classification.

we use the frequency domain data to train a linear support vector machine (SVM) model for texture classification. The dataset of training the SVM is composed by controlling the soft robotic finger to slide each sample fixed on a table 10 times to record the e-skin's output signal at a sampling rate of 1 kHz. In each sliding, a two-second vibration signal associated with the surface textures will be generated, and we split the signal into one-second length signal frames. Overall, 340 s of signal are collected, and 20% of the signal on each texture is randomly selected as a testing set for fivefold cross-validation. The model training is implemented by the MATLAB classification learner toolbox. Since the frequency domain profile is highly representative of textures, the linear SVM can obtain an overall 99% classification accuracy, Fig. 4(e) shows the confusion matrix for classifying all samples.

C. Contents Estimation by Soft Robotic Gripper's Vibration Proprioception

Research on the contents' dynamic behavior in containers is an active topic in physics [32] and robotics (Table S2). After applying motions, the vibration response of a container filled with different contents can differ. In robotic sensing, differentiating content by swinging a container can be achieved by tactile sensors [33], force-torque sensors [34], and acoustic sensors [35], [36]. Inspired by these works, we use the soft robot's vibration proprioception to estimate grain properties by swing the container. The experiment setup is depicted in Fig. 5(a), where two pneumatic soft fingers form a soft gripper to hold a container, and one finger is installed with e-skin for proprioceptive vibration sensing. The soft gripper is installed on the end-effector of a UR3 robotic arm and maintained at 35 kPa positive air-pressure by a proportional valve (Cordis, Clippard) to ensure stable gripping. Fig. 5(b) illustrates the swing motion to agitate the vibration that contains information on the content type and weight, and the swing motion's parameters and trajectory are annotated in Fig. S10. The isotropic symmetric spherical container is adopted to ensure that the container's pose is identical throughout the swing motion.

Previously, frequency profiles from e-skin's output have been used to distinguish the grain type [19] but failed to

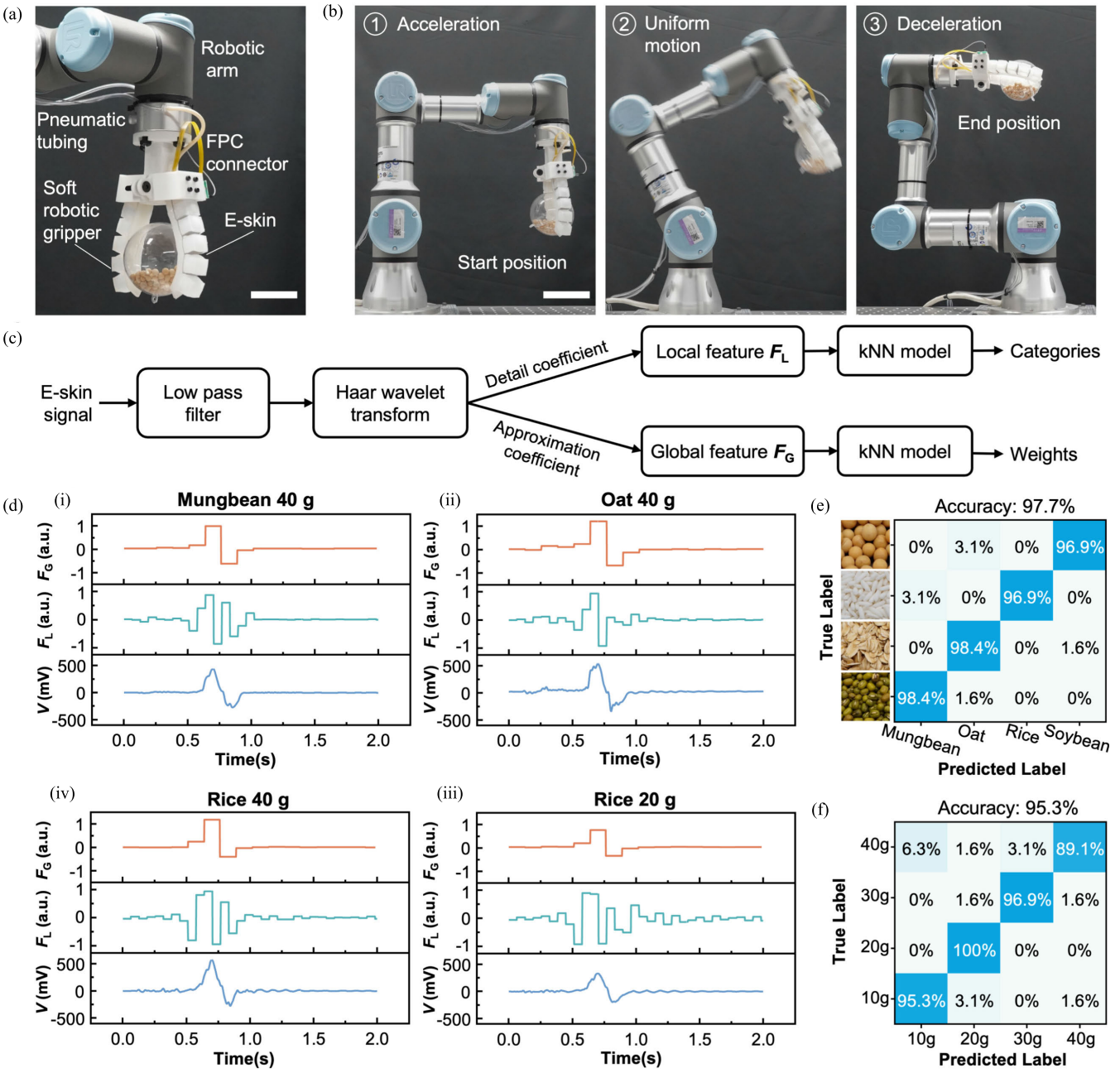

Fig. 5. (a) Experiment setup for grain classification (Scalebar: 5 cm). (b) Swing motion from stage 1: acceleration to stage 2: uniform motion and finally to stage 3: deceleration (Scalebar: 10 cm). (c) Signal processing pipeline. (d) E-skin's output signals (blue line) and their wavelet decomposed local features (F_L) and global features (F_G, red line) of swing grains with different categories and weights (a.u.: arbitrary unit). (e) Confusion matrix of grain categories classification. (f) Confusion matrix of grain weights classification.

differentiate grain weights. Here, a new signal-processing pipeline [see Fig. 5(c)] is introduced to simultaneously estimate grain categories and weights from a single-channel vibration signal. First, the noise from e-skin's output signal is removed by a 40 Hz low-pass filter. Since the grain types affect the frequency domain profile [19], while the grain weights affect the vibration amplitude, the wavelet transform is adopted to decompose different information behind the signal. The wavelet transform-based signal decomposition breaks down the time series signal $x(t)$ by extracting the difference between piecewise constant approximations of the wavelet bases at different scales. The most commonly used orthogonal wavelet bases pair, the Haar wavelet base $\psi(t)$ and its scaling wavelet base $\varphi(t)$ is chosen for wavelet decomposition, which can be formulated as the following equations:

$$\psi_0(t) = \begin{cases} 1, & 0 \le t < 0.5 \\ -1, & 0.5 \le t < 1 \\ 0, & \text{otherwise} \end{cases} \tag{2}$$

$$\varphi_0(t) = \begin{cases} 1, & 0 \le t < 1 \\ 0, & \text{otherwise} \end{cases} \tag{3}$$

The scaled and translated wavelet bases are shown as follows:

$$\psi_{j,n}(t) = 2^{j/2}\psi_0\left(2^j t - n\right) \tag{4}$$

$$\varphi_{j,n}(t) = 2^{j/2}\varphi_0\left(2^j t - n\right) \tag{5}$$

where j is the scale factor, and n is the translation position. The scale factor controls the resolution of the wavelet decomposition, and $j = 7$ is set in the implementation. The detail coefficients ($d_{j,n}$) that capture the signal's local details and the approximation coefficients ($a_{j,n}$) that capture the more general trend of the signal are computed as follows:

$$d_{j,n} = \int x(t)\,\psi_{j,n}(t)\,dt \tag{6}$$

$$a_{j,n} = \int x(t)\,\varphi_{j,n}(t)\,dt. \tag{7}$$

The local feature ($\boldsymbol{F_L}$) for grain categories representation and global feature ($\boldsymbol{F_G}$) for grain weights representation can be calculated as follows:

$$\boldsymbol{F_L} = \sum_n d_{j,n}\psi_{j,n}(t) \tag{8}$$

$$\boldsymbol{F_G} = \sum_n a_{j,n}\varphi_{j,n}(t). \tag{9}$$

Finally, two subspace k-nearest neighbors (kNN) models are used to classify grain categories and weights via the local and global features, respectively.

Fig. 5(d-i)–(d-iii) shows the e-skin's output signals of swinging different grains with the same mass have similar amplitude and global features; however, their local features are distinctive. Fig. 5(d-iii) and (d-iv) compares the signal of swinging the same kind of grain with different weights. It is found that their local features' waveforms are similar, but time domain signal amplitude and global features are different. The plot of e-skin's output signal and their Haar wavelet transform-based decomposed features of all grain type and weight combinations can be found in Fig. S11.

The dataset is composed of swinging each type of grain (mungbean, oat, rice, and soybean) with four weights (10, 20, 30, and 40 g) 20 times, and a two-second data frame during each swing is segmented for wavelet decomposition-based feature extraction. A total of 80% of data from each grain type and weight are randomly selected as a training set and the rest as a testing set. Fig. 5(e) and (f) shows the confusion matrix of using kNN models for grain categories and weights estimation. The overall accuracy of grain categories and weights estimation is 97.7% and 95.3%, respectively.

IV. Conclusion

This work proposes a stretchable e-skin for soft robot proprioceptive vibration sensing. The adoption of the screen-printed LMPs circuit enables the stretchability of the e-skin, making it suitable for integration with stretchable soft robots. Our experimental results demonstrate that the e-skin's output is highly representative of the soft robots' vibration profile and enhances the functionality of soft robots. With vibration proprioception, soft robots can achieve tactile sensing without sensors in direct contact with external samples and achieve content estimation by swinging the container. Looking forward, while our findings highlight the potential of this innovative e-skin in enhancing the perceptual and operational capabilities of soft robots, several challenges remain to be addressed. Future work can improve the durability and robustness of the e-skin by adopting advanced packaging techniques, which allow the e-skin to operate in environments with varying temperatures and humidity. Another area of exploration is to incorporate other sensing mechanisms into the fabrication process of our e-skin. Extending sensor functionality beyond vibration sensing, such as temperature, pressure, and stiffness, is expected to broaden the scope of soft robot capabilities. Additionally, developing adaptive sensing and control algorithms that can accurately interpret increasingly sophisticated signals from multifunctional e-skin and generate optimized decisions for complex robotic systems is also a challenging task. We aim to tackle these challenges in our future work to advance the field of soft robotics, opening new opportunities for research and application that leverage the full potential of stretchable e-skins for multifunctional robotic sensing and interaction.

Acknowledgment

The authors acknowledge Zenan Lin and Xiaosa Li in the setup of vibration exciter.

References

[1] C. M. Boutry et al., "A hierarchically patterned, bioinspired e-skin able to detect the direction of applied pressure for robotics," *Sci. Robot.*, vol. 3, no. 24, Nov. 2018, Art. no. eaau6914.

[2] J. Sinapov, V. Sukhoy, R. Sahai, and A. Stoytchev, "Vibrotactile recognition and categorization of surfaces by a humanoid robot," *IEEE Trans. Robot.*, vol. 27, no. 3, pp. 488–497, Jun. 2011.

[3] Z. Wang, C. Wang, and M. Tomizuka, "Vibration cancellation of semiconductor manufacturing robots," *Manuf. Lett.*, vol. 4, pp. 6–9, Apr. 2015.

[4] H. Wang, M. Totaro, and L. Beccai, "Toward perceptive soft robots: Progress and challenges," *Adv. Sci.*, vol. 5, no. 9, p. 1800541, Sep. 2018.

[5] H. Wu et al., "All-in-one sensing system for online vibration monitoring via IR wireless communication as driven by high-power TENG," *Adv. Energy Mater.*, vol. 13, no. 16, Apr. 2023, Art. no. 2300051.

[6] Y. Zhao et al., "Fully flexible electromagnetic vibration sensors with annular field confinement origami magnetic membranes," *Adv. Funct. Mater.*, vol. 30, no. 25, Jun. 2020, Art. no. 2001553.

[7] E. W. Hawkes, C. Majidi, and M. T. Tolley, "Hard questions for soft robotics," *Sci. Robot.*, vol. 6, no. 53, Apr. 2021, Art. no. eabg6049.

[8] J. C. Yang, J. Mun, S. Y. Kwon, S. Park, Z. Bao, and S. Park, "Electronic skin: Recent progress and future prospects for skin-Attachable devices for health monitoring, robotics, and prosthetics," *Adv. Mater.*, vol. 31, no. 48, Nov. 2019, Art. no. e1904765.

[9] B. Shih et al., "Electronic skins and machine learning for intelligent soft robots," *Sci. Robot.*, vol. 5, no. 41, Apr. 2020, Art. no. eaaz9239.

[10] N. Lu and D.-H. Kim, "Flexible and stretchable electronics paving the way for soft robotics," *Soft Robot.*, vol. 1, no. 1, pp. 53–62, Mar. 2014.

[11] S. Shu, Z. Wang, P. Chen, J. Zhong, W. Tang, and Z. L. Wang, "Machine-Learning assisted electronic skins capable of proprioception and exteroception in soft robotics," *Adv. Mater.*, vol. 35, no. 18, May 2023, Art. no. 2211385.

[12] D. Hu, F. Giorgio-Serchi, S. Zhang, and Y. Yang, "Stretchable e-skin and transformer enable high-resolution morphological reconstruction for soft robots," *Nature Mach. Intell.*, vol. 5, no. 3, pp. 261–272, Feb. 2023.

[13] Z. Shen et al., "High-stretchability, ultralow-hysteresis ConductingPolymer hydrogel strain sensors for soft machines," *Adv. Mater.*, vol. 34, no. 32, Aug. 2022, Art. no. e2203650.

[14] T. G. Thuruthel, B. Shih, C. Laschi, and M. T. Tolley, "Soft robot perception using embedded soft sensors and recurrent neural networks," *Sci. Robot.*, vol. 4, no. 26, Jan. 2019, Art. no. eaav1488.

[15] T. Li, J. Guo, Y. Tan, and Z. Zhou, "Recent advances and tendency in fiber Bragg grating-based vibration sensor: A review," *IEEE Sensors J.*, vol. 20, no. 20, pp. 12074–12087, Oct. 2020.

[16] B. S. Athira et al., "High-performance flexible piezoelectric nanogenerator based on electrospun PVDF-$BaTiO_3$ nanofibers for self-powered vibration sensing applications," *ACS Appl. Mater. Interfaces*, vol. 14, no. 39, pp. 44239–44250, Oct. 2022.

[17] H. Zhao et al., "A highly sensitive triboelectric vibration sensor for machinery condition monitoring," *Adv. Energy Mater.*, vol. 12, no. 37, Oct. 2022, Art. no. 2201132.

[18] Y. Cheng et al., "Highly stretchable triboelectric tactile sensor for electronic skin," *Nano Energy*, vol. 64, Oct. 2019, Art. no. 103907.

[19] Z. Wang et al., "STEV: Stretchable triboelectric E-skin enabled proprioceptive vibration sensing for soft robot," in *Proc. IEEE Int. Conf. Robot. Autom. (ICRA)*, London, U.K., May 2023, pp. 588–593.

[20] S. Niu et al., "Theoretical investigation and structural optimization of single-electrode triboelectric nanogenerators," *Adv. Funct. Mater.*, vol. 24, no. 22, pp. 3332–3340, Jun. 2014.

[21] H. Zou et al., "Quantifying the triboelectric series," *Nature Commun.*, vol. 10, no. 1, p. 1427, Mar. 2019.

[22] Y.-L. Park, B.-R. Chen, and R. J. Wood, "Design and fabrication of soft artificial skin using embedded microchannels and liquid conductors," *IEEE Sensors J.*, vol. 12, no. 8, pp. 2711–2718, Aug. 2012.

[23] M. D. Dickey, R. C. Chiechi, R. J. Larsen, E. A. Weiss, D. A. Weitz, and G. M. Whitesides, "Eutectic gallium-indium (EGaIn): A liquid metal alloy for the formation of stable structures in microchannels at room temperature," *Adv. Funct. Mater.*, vol. 18, no. 7, pp. 1097–1104, Apr. 2008.

[24] Y. Lin, J. Genzer, and M. D. Dickey, "Attributes, fabrication, and applications of gallium-based liquid metal particles," *Adv. Sci.*, vol. 7, no. 12, Jun. 2020, Art. no. 2000192.

[25] L. Tang, J. Shang, and X. Jiang, "Multilayered electronic transfer tattoo that can enable the crease amplification effect," *Sci. Adv.*, vol. 7, no. 3, Jan. 2021, Art. no. eabe3778.

[26] S. Liu et al., "Laser sintering of liquid metal nanoparticles for scalable manufacturing of soft and flexible electronics," *ACS Appl. Mater. Interfaces*, vol. 10, no. 33, pp. 28232–28241, Jul. 2018.

[27] H. Wang et al., "A highly stretchable liquid metal polymer as reversible transitional insulator and conductor," *Adv. Mater.*, vol. 31, no. 23, Jun. 2019, Art. no. e1901337.

[28] W. Lee et al., "Universal assembly of liquid metal particles in polymers enables elastic printed circuit board," *Science*, vol. 378, no. 6620, pp. 637–641, Nov. 2022.

[29] L. Tang et al., "Printable metal-polymer conductors for highly stretchable bio-devices," *iScience*, vol. 4, pp. 302–311, Jun. 2018.

[30] B. Mosadegh et al., "Pneumatic networks for soft robotics that actuate rapidly," *Adv. Funct. Mater.*, vol. 24, no. 15, pp. 2163–2170, 2014.

[31] Z. Song et al., "A flexible triboelectric tactile sensor for simultaneous material and texture recognition," *Nano Energy*, vol. 93, Mar. 2022, Art. no. 106798.

[32] S. Nadler, O. Bonnefoy, J.-M. Chaix, G. Thomas, and J.-L. Gelet, "Parametric study of horizontally vibrated grain packings: Comparison between discrete element method and experimental results," *Eur. Phys. J. E*, vol. 34, no. 7, p. 66, Jul. 2011.

[33] X. Guo, H.-J. Huang, and W. Yuan, "Estimating properties of solid particles inside container using touch sensing," presented at the IEEE/RSJ Int. Conf. Intell. Robots Syst. (IROS), Detroit, MI, USA, Oct. 2023.

[34] C. Matl, R. Matthew, and R. Bajcsy, "Haptic perception of liquids enclosed in containers," in *Proc. IEEE/RSJ Int. Conf. Intell. Robots Syst. (IROS)*, Macau, China, Nov. 2019, pp. 7142–7149.

[35] M. Eppe, M. Kerzel, E. Strahl, and S. Wermter, "Deep neural object analysis by interactive auditory exploration with a humanoid robot," in *Proc. IEEE/RSJ Int. Conf. Intell. Robots Syst. (IROS)*, Madrid, Spain, Oct. 2018, pp. 284–289.

[36] S. Jin, H. Liu, B. Wang, and F. Sun, "Open-environment robotic acoustic perception for object recognition," *Frontiers Neurorobotics*, vol. 13, p. 96, Nov. 2019.

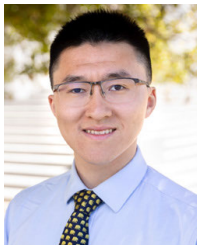

Zihan Wang received the dual B.Eng. (Hons.) degrees from Xidian University, Xi'an, China, and Heriot-Watt University, Edinburgh, U.K., in 2019. He is currently pursuing the Ph.D. degree in data science and information technology with Tsinghua University, Beijing, China.

He is a Visiting Student Researcher with the University of California at Berkeley, Berkeley, CA, USA. His research interests focus on intelligent sensory systems with their applications in soft robots and wearable electronics.

Kai-Chong Lei received the B.Eng. and B.B.A. degrees from Shanghai Jiao Tong University, Shanghai, China, in 2021. He is currently pursuing the M.Eng. degree in artificial intelligence with the Smart Sensing and Robotics (SSR) Group, Tsinghua–Berkeley Shenzhen Institute, Tsinghua University, Beijing, China.

His research interests include soft robotics, smart materials, stretchable electronics, and self-powered sensing.

Huaze Tang (Graduate Student Member, IEEE) received the B.S. degree in communication engineering from Southeast University, Nanjing, China, in 2021. He is currently pursuing the Ph.D. degree in data science and information technology with the Smart Sensing and Robotics (SSR) Group, Tsinghua University, Beijing, China.

His research interests focus on signal processing with deep learning, reinforcement learning, and soft robots.

Yang Luo received the bachelor's degree from Northeastern University, Shenyang, China, in 2019, and the master's degree from Tsinghua University, Beijing, China, in 2022.

His current research interests include reconfigurable surfaces and flexible haptics.

Hongfa Zhao received the B.S. and M.S. degrees in marine engineering from Dalian Maritime University, Dalian, China, in 2018 and 2021, respectively. He is currently pursuing the Ph.D. degree in data science and information technology with Tsinghua–Berkeley Shenzhen Institute, Tsinghua University, Beijing, China.

His research interests mainly focus on the design and theoretical analysis of triboelectric nanogenerators.

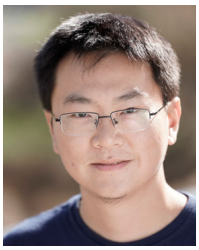

Peisheng He received the B.S. degree in materials science and engineering from Shanghai Jiao Tong University, Shanghai, China, in 2018, and the M.S. and Ph.D. degrees in mechanical engineering from the University of California at Berkeley, Berkeley, CA, USA, in 2020 and 2023, respectively.

He is currently a Postdoctoral Research Fellow with the University of California at Berkeley under the Supervision of Prof. Liwei Lin. His research interests focus on soft multifunctional materials and their applications for stretchable electronics in sensing, muscle-like actuation, and energy storage.

Wenbo Ding (Member, IEEE) received the B.S. and Ph.D. (Hons.) degrees from Tsinghua University, Beijing, China, in 2011 and 2016, respectively.

He was a Postdoctoral Research Fellow with Georgia Tech, Atlanta, GA, USA, under the supervision of Prof. Z. L. Wang from 2016 to 2019. He is now an Associate Professor and a Ph.D. supervisor with Tsinghua–Berkeley Shenzhen Institute, Tsinghua Shenzhen International Graduate School, Tsinghua University, where he leads the Smart Sensing and Robotics (SSR) Group. His research interests include mechanosensing, tactile sensing, and robotics with the help of signal processing and machine learning.

Dr. Ding has received many prestigious awards, including the Gold Medal of the 47th International Exhibition of Inventions Geneva and the IEEE Scott Helt Memorial Award.

Liwei Lin (Member, IEEE) received the B.S. degree in mechanical engineering from the Power Mechanical Engineering Department, National Tsing Hua University, Hsinchu, Taiwan, in 1986, and the M.S. and Ph.D. degrees in mechanical engineering from the Mechanical Engineering Department, University of California at Berkeley (UC Berkeley), Berkeley, CA, USA, in 1991 and 1993, respectively.

He is currently the James Marshall Wells Professor with the Department of Mechanical Engineering and the Co-Director of the Berkeley Sensor and Actuator Center, UC Berkeley. He has authored or coauthored more than 300 journal articles. His research interests include microelectromechanical systems (MEMS), nanoelectromechanical systems, nanotechnology, design and manufacturing of microsensors and microactuators, development of micromachining processes by silicon surface/bulk micromachining, micromolding process, and mechanical issues in MEMS, such as heat transfer, solid/fluid mechanics, and dynamics.

Dr. Lin is a Fellow of ASME.